A79-35110

NASA TECHNICAL MEMORANDUM NASA TM -75799

FIRST RESULTS OF A STUDY ON TURBULENT BOUNDARY LAYERS IN OSCILLATING FLOW WITH A MEAN ADVERSE PRESSURE GRADIENT

R. Houdeville and J. Cousteix

(NASA-TM-75799) FIRST RESULTS OF A STUDY ON TURBULENT BOUNDARY LAYERS IN OSCILLATING FLOW WITH A MEAN ADVERSE PRESSURE GRADIENT (National Aeronautics and Space Administration) 37 p HC A03/MF A01 CSCL 20D G3/34

N80-17400

Unclas 47230

Translation of "Premiers Résultats d'Une Étude sur les Couches Limites Turbulentes en Écoulement Pulsé avec Gradient de Pression Moyen Défavorable," 15e Colloque D'Aérodynamique Appliquée, Marseille, 7 - 8 and 9 November 1978

pp 1-16

NATIONAL AERONAUTICS AND SPACE ADMINISTRATION
WASHINGTON, D.C. 20546 NOVEMBER 1979

STANDARD TITLE PAGE

1. Report No. NASA TM-75799	2. Government Accession No.	3. Recipient's Catalog No.
4. Title and Subtitle FIRST RESULTS OF A STUDY ON TURBULENT BOUNDARY LAYERS IN OSCILLATING FLOW WITH A MEAN ADVERSE PRESSURE GRADIENT		5. Report Date November 1979 6. Performing Organization Code
7. Author(s) A. Houdeville and J. Cousteix Office National d'Etudes et de Recherches Aérospatiales (ONERA) CERT, Toulouse (France)		8. Performing Organization Report No. 10. Work Unit No.
9. Performing Organization Name and Address Leo Kanner Associates Redwood City, California 94063		11. Contract or Grant No. NASw-3199 13. Type of Report and Period Covered Translation
12. Sponsoring Agency Name and Address National Aeronautics and Space Administration, Washington, D.C. 20546		14. Sponsoring Agency Code

15. Supplementary Notes Translation of "Premiers Résultats d'Une Étude sur les Couches Limites Turbulents en Écoulement Pulsé Avec Gradient de Pression Moyen Défavorable," 15e Colloque D'Aérodynamique Appliquée, Marseille, 7-8 and 9 November 1978, pp 1-16 (A79-35110)

16. Abstract A study of the development of a turbulent unsteady boundary layer with a mean pressure gradient strong enough to induce separation, in order to complete and extend results obtained for the flat plate configuration. The longitudinal component of the velocity is measured using constant temperature hot wire anemometer. The region where negative velocities exist is investigated with a laser Doppler velocimeter system with BRAGG cells. The boundary layer responds by forced pulsation to the perturbation of potential flow. The unsteady effects observed are very important. The average location of the zero skin friction point moves periodically at the perturbation frequency. Average velocity profiles from different instants in the cycle are compared. The existence of a logarithmic region enables a simple calculation of the maximum phase shift of the velocity in the boundary layer. An attempt of calculation by an integral method of boundary layer development is presented, up to the point where reverse flow starts appearing.

17. Key Words (Selected by Author(s))	18. Distribution Statement
	Unclassified-Unlimited

19. Security Classif. (of this report)	20. Security Classif. (of this page)	21. No. of Pages	22. Price
Unclassified	Unclassified	37	

FIRST RESULTS OF A STUDY ON TURBULENT BOUNDARY LAYERS IN OSCILLATING FLOW WITH A MEAN ADVERSE PRESSURE GRADIENT

by R. Houdeville and J. Cousteix

Summary

The development of a turbulent unsteady boundary layer with a /1* mean pressure gradient, strong enough to induce separation, is studied in order to complete and extend the results obtained for the flat plate configuration.

The longitudinal component of the velocity is measured using constant temperature hot wire anemometer. The investigation of the region where negative velocities exist is performed with a laser Doppler velocimeter system with BRAGG cells.

As in the flat plate configuration, the boundary layer responds by a forced pulsation to the perturbation of the potential flow. Due to the experimental conditions, the unsteady effects are very important; for example, the average location of the zero skin friction point moves periodically at the perturbation frequency.

The study of the longitudinal component of turbulence deals with its standard deviation as well as its moments of order 3 and 4 which give some information about the development of turbulence.

The comparison of average velocity profiles, obtained at different instants in the cycle, with profiles deduced from similarity solutions shows a good agreement up to values of the shape parameter close to the separation value. Moreover, the existence of a logarithmic region enables a simple calculation of the maximum phase shift of the velocity in the boundary layer.

To conclude, an attempt of calculation by an integral method of the boundary layer development is presented, up to the point where reverse flow starts appearing.

1-INTRODUCTION

---

*Numbers in the margin indicate pagination in the foreign text.

The study of flat plane boundary layers subjected to periodic oscillating flows is mainly conducted in the reduced frequency range which is not too high. If such experiments allow for the definition of a certain number of important theoretical data, they must nevertheless be quite far from practical cases encountered in unsteady aerodynamic problems encountered, for example, the problem of the dynamic jitter of a helicopter blade.

In order to approach such a situation and also to provide experimental data required for the development of calculation methods, we shall study the development of a pulsated boundary layer with a positive mean pressure gradient which may lead to separation. The experimental study deals mainly with the longitudinal component of velocity as well as with its fluctuating components characterized by its standard deviation and its higher moments.

2 - EXPERIMENTAL CONDITIONS

2.1. - Experimental Device

A turbulent boundary layer subjected to a pulsating external flow is developed on the floor of a test section which is rectangular: 160 x 220 mm. Abrasive paper, glued 100 mm ahead of the inlet of the test section along a length of 105 mm in the collector of the wind tunnel allows the transition to be triggered and measured.

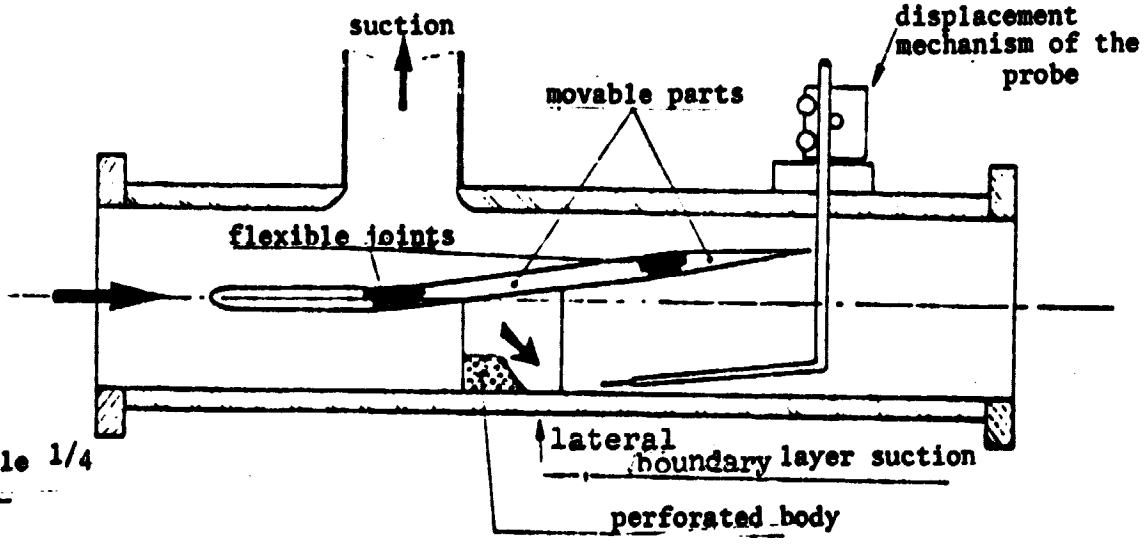

Figure 1. Diagram of experimental assembly

Upstream from the study section is located a swirl vane, the rotation of which induces the flow pulsation by changing the total pressure loss of the aerodynamic circuit.

A streamlined body, composed of rigid parts interconnected among each other by flexible connections, induces on the floor of the test section a longitudinal mean pressure gradient which is adjustable. Suction of part of the higher rate of flow prevents blocking from taking place toward the trailing edge of the main body, as this would induce /2 considerable overvelocities on the floor at the test section inlet. A correct adjustment of the upper suction area equalizes the pressures of the streamlined body at the test section inlet.

To prevent a separation of the lateral boundary limits and, hence, spurious tridimensional effects, a suction of these lateral boundary layers is produced in a region located upstream from the one where the unsteady separation occurs, which is the objective of this study, which permits the passage of the light beams from the laser anemometer. Visualizations of the parietal streamlines, which are performed in an unsteady state with a mixture of oil and black smoke have made it possible to state that it was possible to obtain an average two dimensional flow over about half of the space across the test section and over a length exceding 600 mm.

As previous studies have demonstrated the detrimental effect of the presence of static pressure intakes on the development of a boundary layer in unsteady state, none have been placed on the floor in the measuring region.

Considering the extreme vibratory environment, particular attention has been brought to the attachment of the test section. For example, the translation mechanism of the measuring centers is not mechanically connected to the wind tunnel, but is attached to a stable support fixed directly on the ground. With these precautions taken into account, there is no visible evidence of vibration of the measuring sensors, nor of the floor of the test section from the sighting telescope.

2.2. - Methods of measuring. Data processing.

The measurement of instantaneous velocities is performed in a

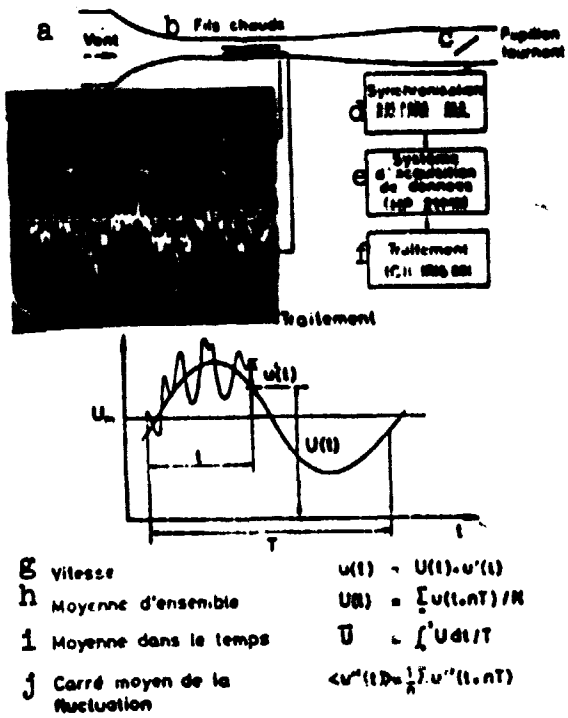

Figure 2. System of acquisition and treatment of data

Key:
a) wind
b) hot wires
c) rotating butterfly valve
d) synchronization
e) system of data acquisition
f) treatment
g) velocity
h) overall average
i) time average
j) mean square fluctuation

standard manner with the use of DISA 55 M type hot wire anemometer with a constant temperature. The range of application of the hot wire was limited to positive speed flows, the use of the laser anemometer has made it possible to measure the velocity in regions where there are return flows.

The velocimeter used, of the Doppler type, was developed at ONERA [1-2]; we shall review briefly its operating principle. A coherent light beam ($\lambda = 514.5$ mm) of 2.8 watts emitted by a nitrogen laser source is divided into two parallel beams of equal intensity symmetrical in relation to the measuring volume; this is carried out with the use of two BRAGG cells, located behind the beam divider, which separates the light ray frequencies of 200 and 204 MHz respectively. The interband, about 7.85 μm, was determined by the measuring volume on a photomultiplier. There is no special problem concerning space requirement in the case of our mounting, diffusion takes place toward the front. The processing of the Doppler signal is done using a DISA 55L90 computer, directly connected to a Hewlett Packard 21 MX computer through its digital output. The two windows having dimensions of 200 x 100 mm, are made of antiglare treated glass with an evenness of 10 λ along their longest length.

Technique of measurement analysis

/3

As the flow is periodic and turbulent, a statistical analysis of data is required to separate the average component of velocity from the turbulent part. To accomplish this each cycle is considered as the occurence of the same phenomenon; the averages, i.e. overall averages, are computed by always placing the various successive periods in the same phase. The phase data is provided by the rotation of the swirl vane which induces the periodic flows. This rotation generates, through a photo-electric cell, a series of impulses which always correspond to the specified values of the phase angle. The signal from the hot wire anemometer is digitized at each impulse; we have, then, the velocity of 24 moments in each cycle.

In the case where the laser velocimeter is used, the procedure is a little more delicate, as in principle the velocity data is sampled and supplied randomly in time. The measured speed is the last value at the counter prior to the corresponding impulse. In order to effectively obtain the velocity at a given phase and not an average over $1/24^{th}$ of a cycle, which would systematically result in substantial errors, for example, in the rate of turbulence, the flow is seeded with sensor particles in order to insure very high measuring rate at the counter which would exceed 50,000 measurements per second, corresponding to an average lag between two measurements of less than $1/1000^{th}$ of a cycle. In the relatively improbable case where no particle passes into the measuring volume between two impulses, the value computed by the counter is not taken into account.

By definition, the random fluctuation of the velocity u' has an overall average of zero. u' is obtained by the difference between the overall average of the velocity U and its instantaneous value. u' may then be analyzed by using its standard deviation $\langle u'^2 \rangle^{1/2}$ or its moments of higher orders.

In order to obtain a certain accuracy for the values of U or for $\langle u'^2 \rangle$, averages must be calculated from a sufficient number of results; we have selected to work with 600 or 1200 cycles depending on the rate of turbulence. We shall estimate the accuracy thus obtained from the statistical theory of errors. The law of large numbers indicates in

fact that if $X_1, X_2 \ldots, X_n$ are the values taken by a random variable X during n independent computations, whereas when $n \to \infty$, the variable $\sum x_i/n$ leads to a random variable which follows a standard deviation law $\sigma/\sqrt{n}$ where σ is the standard deviation of X; m being the mean value of X: $\sigma = \sqrt{(x-m)^2}$. We have then:

$$P\left[\left|\frac{\sum_1^n x_i}{n} - m\right| < h\right] = \frac{2}{\sqrt{2\pi}} \int_0^{\frac{h\sqrt{n}}{\sigma}} e^{-t^2} dt$$

The accuracy obtained for the mean velocity U by $U = \Sigma u_i/n$ can be calculated if it is given that the probability of error is below h; with $P = 0.9$, we have then: $\frac{h\sqrt{n}}{\sigma} = 1{,}64$

Let us assume the following conditions:

$\frac{\sqrt{\langle u'^2 \rangle}}{U} = 15\ \%$ $\quad n = 600$ (region quite far from the separation) (1)

$h = 7\ ^0/_{00}$

$\frac{\sqrt{\langle u'^2 \rangle}}{U} = 50\ \%$ $\quad n = 1200$ (region near the separation) (2)

$h = 2{,}4\ \%$

The determination of the accuracy on the turbulence rate is obtained in a similar manner, X_i represents now the standard deviation of the velocity. Let us compute the standard deviation of X_i :

$$\sigma_{x_i}^2 = \frac{1}{n}\left(\sum_1^n u_i'^2 - \langle u'^2 \rangle\right)^2 = \langle u'^4 \rangle - \langle u'^2 \rangle^2$$

If we assume a Gaussian distribution for the turbulence, we have then:

$$\frac{\langle u'^4 \rangle}{\langle u'^2 \rangle^2} = 3 \qquad \text{and} \qquad \frac{\sigma_{x_i}^2}{m^2} = 2$$

Always with a probability of 0.9, the error made on the turbulence rate is given by:

$$\frac{h\sqrt{n}}{\sqrt{2}} = 1{,}64$$

It may be observed that it is independent from the turbulence level.

For n = 600 and 1200, we have then h = 10% and 7% respectively.

It would have been possible, of course, to use more points in order to insure a better accuracy. However, it should be observed that it increases as $\sqrt{n}$, or 1200 points which represent data acquisition during one minute for a simple point of the boundary layer.

The computations made above for estimating the measurement accuracy depend on the independence of the various results; if account is taken of the relatively large difference between the oscillating frequency and the characteristic turbulence frequencies, it may be considered that this last condition has been accomplished, especially since the averages are computed every 2 cycles.

2.3. - Laser velocimeter - hot wire comparison.

Before beginning the presentation of the experimental results, we shall make a comparison between the measurements made with the laser velocimeter and the hot wire in the same conditions used for our experiment; for example, we use the BRAGG cells, even though they are not indispensible in this particular case. To accomplish this we shall place a station at 435 mm from the test section inlet where return flows never occur.

Treatment of the data processed by the laser velocimeter is the same as for measurements made with the hot wire; overall averages are computed by selecting a given phase in the cycle; as the rate of particle flow is high for such sampling no correction is required to compute the averages. On the other hand only the data located in the standard deviation interval $\pm$ 5 are taken into account; it is important not to reduce this interval in order to avoid the likelihood of making a large error in the calculation of the moments of orders 3 and 4 of the speed fluctuation. Finally, it is necessary to define the size of the measuring volume, limited by the diaphragm located in front of the photomultiplier, which is 0.3 mm; as the boundary layer thickness is more than 30 mm, the error in calculating the moments with even degrees by the average speed gradient in the measuring values is small /4 compared to other causes of error, it is thus not necessary to make a correction in the calculation of these moments.

In figure 3 we shall compare the evolution as a function of time of the mean velocity relative to its continuous component; this is performed in the boundary layer at various distances from the skin and 1200 cycles are used for this measurement.

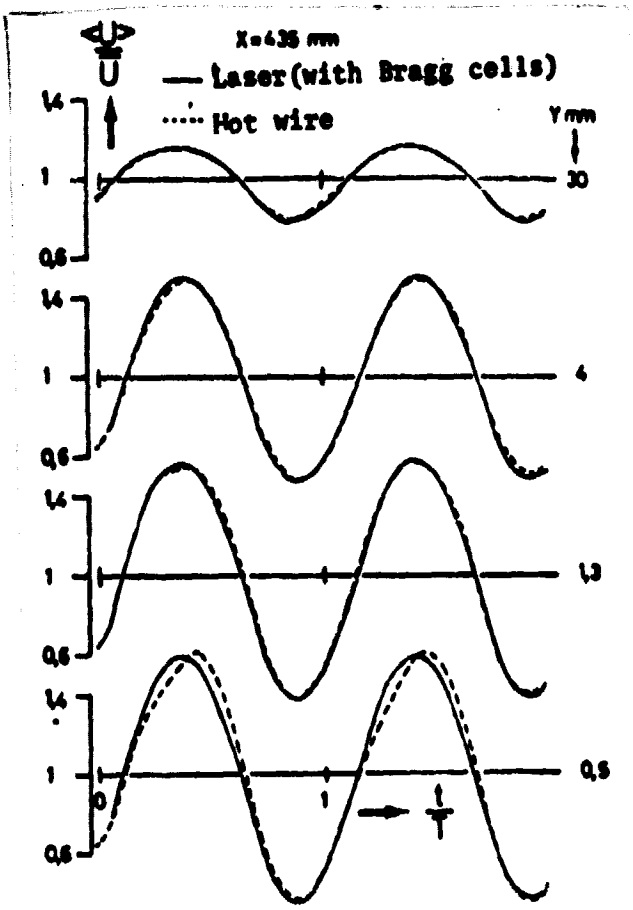

Figure 3. Anemometer comparison of laser-hot wire. Mean velocity.

The deviations observed are small and are not significant; in fact, for practical reasons, it was not possible to make estimates during a single test by placing the hot wire just behind the measuring volume of the velocimeter.

The turbulence intensity profiles, obtained at three different instants in the cycle (Fig. 4) show a satisfactory agreement. It should nevertheless be observed that the laser velocimeter always indicates an excessive turbulence rate outside the boundary layer; this comes from a limitation in the counter efficiency, with the accuracy of each individual measurement being about 1.5%.

To extend our comparison further we present in Fig. 5 the evolution of the dissymetrical and flattening factors in the boundary layer at a given instant in the cycle. The good agreement observed would not have been obtained if we had to eliminate in the case of the laser velocimeter the velocity values outside of the interval $\pm$ 2.5 or 3 σ ; this was made possible due to the good quality of the Doppler signals and to the effectiveness of the circuits eliminating incorrect counter measurements.

As the coherence of the two measuring methods used, laser velocimeter and hot wire, was established within the framework of our study, we shall not define in the presentation which follows the experimental results the measuring method used. Let us add only that the

probes of the boundary limits performed up to the location x = 390 mm have been measured with the hot wire, the laser velocimeter then took its place. The external velocity was especially measured with the hot wire.

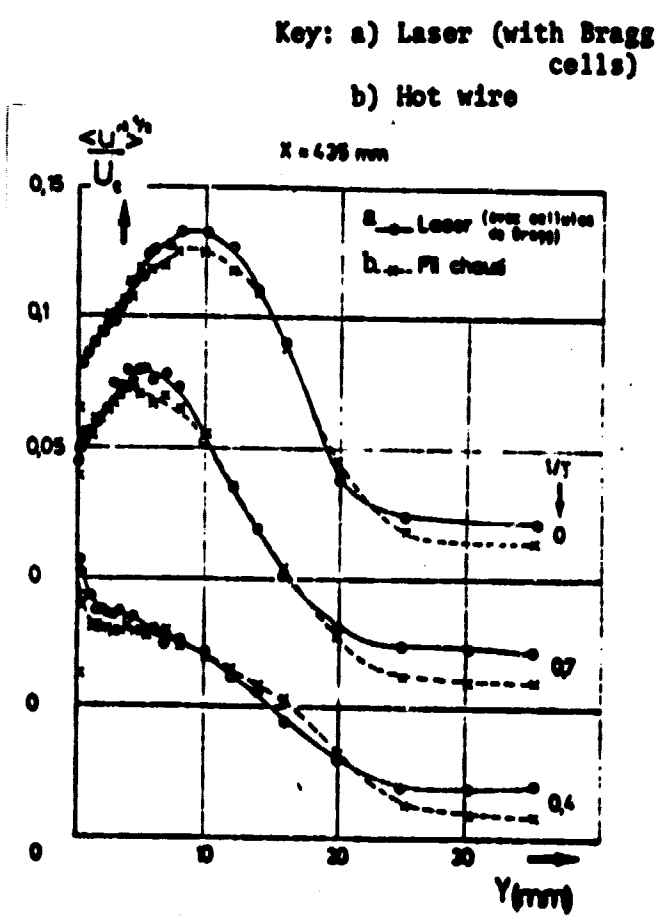

Figure 4. Anemometer comparison of laser-hot wire. Turbulence.

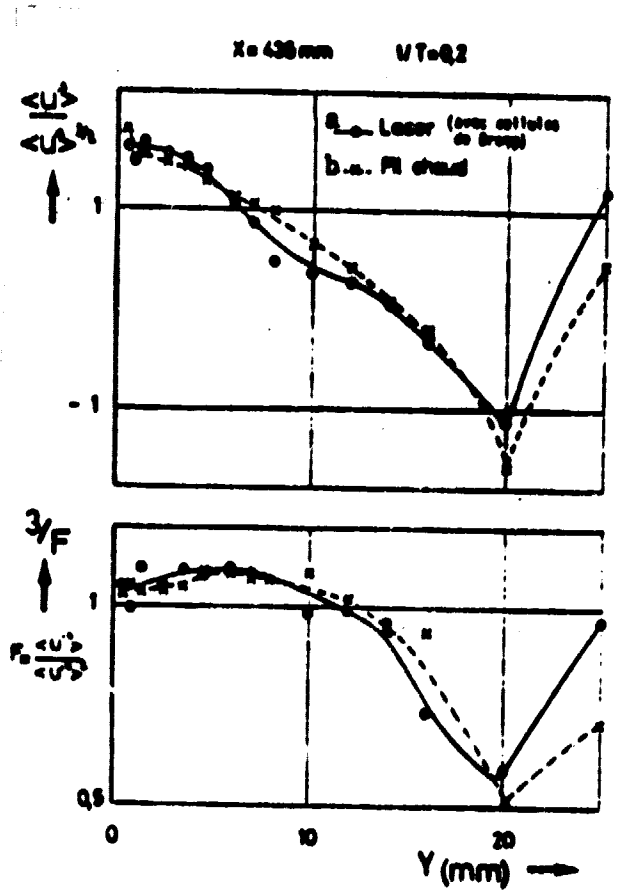

Figure 5. Anemometer comparison of laser-hot wire. Dissymetry factor and flattening.

3 - EXPERIMENTAL RESULTS

3.1. - External velocity

As we have seen the pulsation of the flow is created by the rotation of the swirl vane located upstream from the test section. It may be observed that there is a resonance frequency for which the pulsation is practically sinusoidal. The entire study presented is made of this special frequency equal to 38 Hz.

The harmonic analysis of the external velocity limited to the fundamental frequency is presented in figure 6. The harmonics of higher order remain low, below 10% of the fundamental value, except

upstream from the region with the return flow (X > 550 mm) where they become quite high.

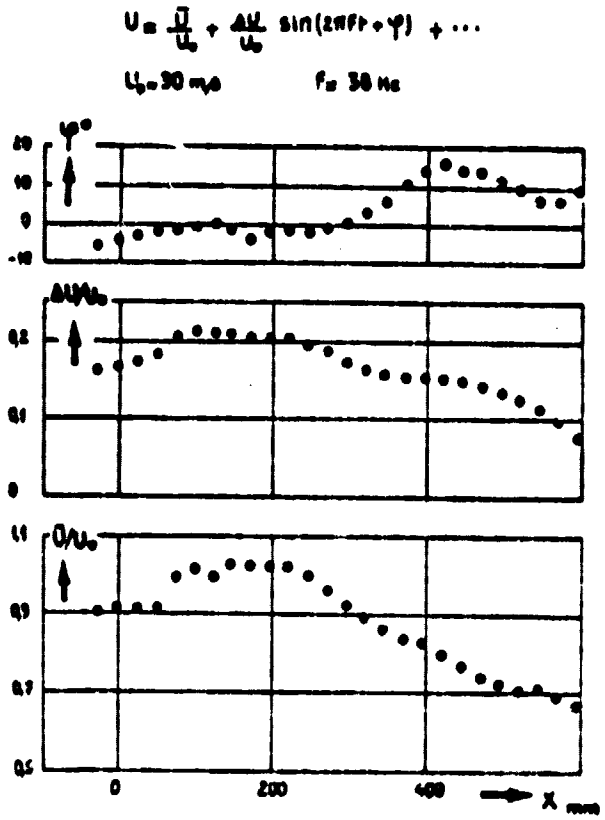

Figure 6. Harmonic analysis of exterior velocity.

The continuous component of velocity, close to 27 m/s at the test section inlet, increases up to 30 m/s in the region of the constant section under the streamlined body; this velocity increase comes simply from the decrease in this section due to the main body. It may be observed that it would be considerably higher without the suction of one part of the flow rate passing above the obstacle. After X = 200 mm, the divergence of the channel creates a constant decrease in the continuous component.

The variation amplitude, approximately 20% of U_o at the test section inlet, decreases considerably as it moves farther upstream; it should nevertheless be observed that the relative fluctuation amplitude, ie the one related to the local continuous component, remains essentially constant and ranges between 15 and 20%.

The phase angle remains low with a slight increase in the decelerated part of the flow in addition to the Reynolds number which remains an essential parameter to characterize the flow, other parameters must be considered in the unsteady flow. Among the most important ones, we shall draw to attention the Strouhal number $X\omega = \omega X/U_{m3}$ the relative fluctuation amplitude of the external velocity: $\Delta U_e/U_e$, the frequency of the periodic flow ω and a characteristic turbulence frequency $f_e = u'/\delta$. As the study of the boundary layers is carried out on the floor of the test section, the length X is counted from a fictive origin of the turbulent boundary layer determined by using a flat plate law for the mean flow. The table below defines the values of the various parameters. For the calculation of f_t the characteristic velocity u' of the turbulence

under consideration is taken as equal to the mean value of $\overline{\omega' v'}$, next to the skin. This frequency is considerably higher then the periodic frequency of the flow, except in the vicinity of the region where the negative velocities exist; we may then expect a certain interaction of the pulsation on the development of turbulence and therefore more accentuated unsteady effects in this region.

3.2. - Integral values

X geometric	$\frac{\Delta U_e}{U_e}$	$10^{-6}\frac{X U_{max}}{\nu}$	$\frac{\omega X}{U_{max}}$	f_e
100	0,19	0,74	3,0	350
240	0,16	0,91	4,6	300
390	0,16	1,00	7,0	230
604	0,13	1,15	10,0	70

Observation of the development of displacement thickness and of the shape parameter as a function of time at various locations depending on X permits a first global description of the development of the boundary layer and of the beginning of separation. Figure 7 shows a substantial increase in the mean displacement thickness as the location of the probe recedes; between the extreme locations studied, the mean value of δ_1 goes from 1.5 to 18 mm. In the upstream parts of the zone under study δ_1 varies in a steady manner as a function of time, with only a very small variation from a sinusoid; the same is the case for the shape parameter H (Fig.8). Furthermore, δ_1 and H are practically in phase opposition in relation to the external velocity; the boundary layer thickness passes through a maximum when the velocity is low. This has already been observed during studies performed on the flat plate configuration without the mean pressure gradient [3-4-9].

The unsteady effects seem to increase when one moves upstream, it may be observed in fact that the variations of H and of δ_1 are increasingly larger. This may be explained by observing, as we shall see later on during the study of similarity solutions, that the pressure gradient parameter due to the flow fluctuation has the shape $-\frac{\delta}{\rho U_m^2}\frac{\partial}{\partial x}\frac{\partial U_m}{\partial t}$; /6 this term is larger as the boundary layer is thicker and the parietal friction is lower, i.e. when we approach the region of separation.

It is not easy to locate at each instant the zero friction point; for example if we consider that $c_f = 0$ corresponding to a value of the shape parameter close to 2.6 (5), it may be observed that a further location of the zero friction point is close to 450 mm. The displacement amplitude of this point is quite high as at the last location of this

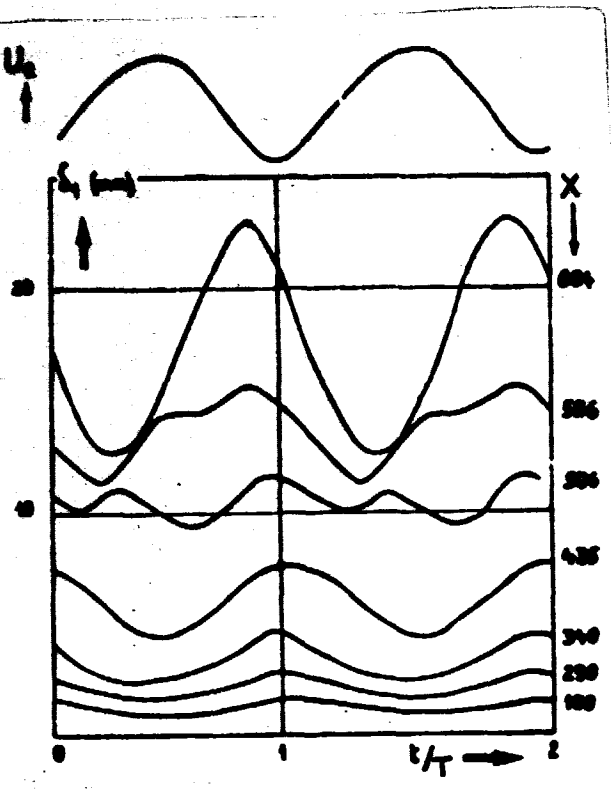

Figure 7. Thickness of displacement.

measurement (X = 604 mm), there are still instants in the cycle where H remains less than 2.6. The presence of considerable harmonics may also be observed in this region, as well as for δ_1 and for H; these harmonics disappear toward the upstream region.

3.3. - Harmonic analysis of velocity in the boundary layer

The study of unsteady effects on the boundary layer profiles may be carried out on the basis of the harmonic analysis of velocity. As the latter is almost sinusoidal, we are interested only in the first harmonic.

The continuous velocity component profiles shown in figure 9 for the various locations depending on X do not demonstrate any special characteristics showing a large difference compared to the unsteady boundary layer profiles. This confirms a fact already observed in the case of a flat plate configuration, mainly the low effect of the nonlinear equation terms on the development of the average boundary layer component.

The amplitude fluctuation profiles reduced by the external velocity fluctuation, are shown in figure 10 at various abscissas. The locations X = 100 and 196 mm correspond to a region where the mean velocity gradient is zero; the excessive amplitude in the boundary layer, less than 10%, is similar to what has been observed by various authors for such a configuration [3-9]. The positive mean pressure gradient begins to act after X = 220 mm which is shown on the amplitude profiles by considerable increase in the excess of ΔU_e near the skin which could reach nearly 60% at X = 390 mm. Also observed toward the outside of the boundary layer are values of the relative amplitude considerably lower than 1.

The phase angle profiles develop more as one moves upstream, i.e.

when the mean pressure gradient is higher. For sensor locations farther back no more positive phase angles are observed near the skin.

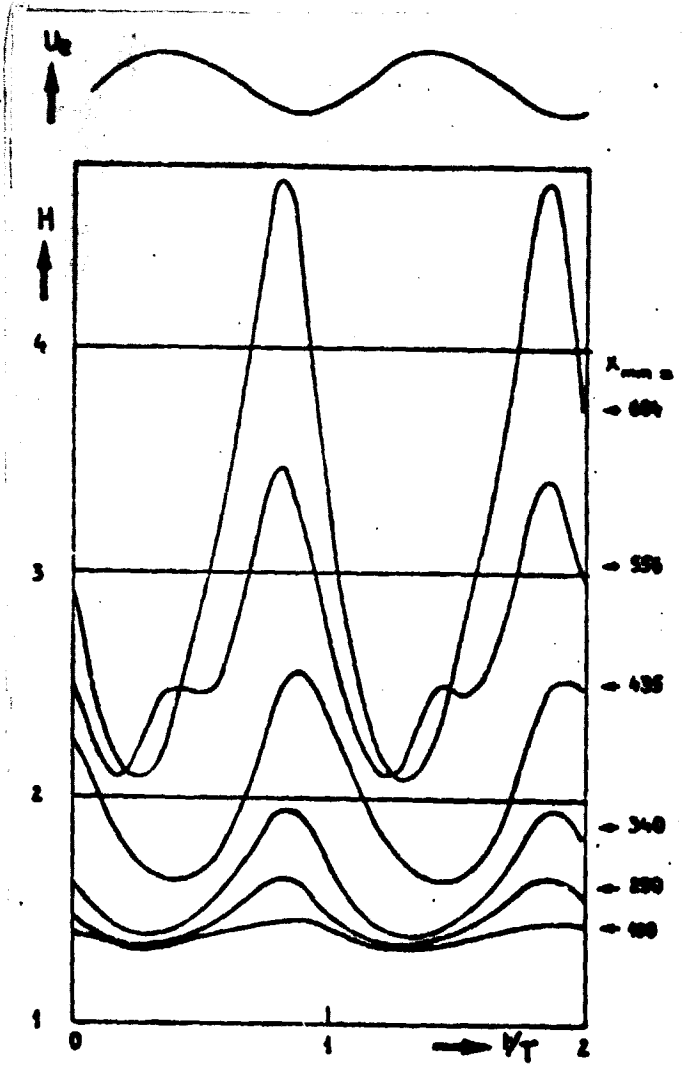

Figure 8. Shape parameter.

3.4. - Mean velocity profiles. Study of turbulence. /8

After describing the overall evolution of the velocity profiles according to X, we shall now present the same profiles but fixed at various instants in the cycle, and that for two measuring locations. These profiles, as well as the turbulence intensity profiles, have been estimated as overall averages from 600 and 1200 cycles for the stations 240 and 604 mm respectively (Figs. 12 and 13).

At station x = 240 mm, i.e. at the location where the mean pressure gradient begins to move, the velocity profile varies moderately over the cycle, as the boundary layer is subjected to an instantaneous variable pressure gradient. The effect of this gradient is easier to observe on the evolution of turbulence profiles (Fig. 12), their shape presents at instant 21 a pattern similar to the one observed for an unsteady boundary layer which is slightly decelerated.

The location of station 604 mm is very different (Fig. 13) at

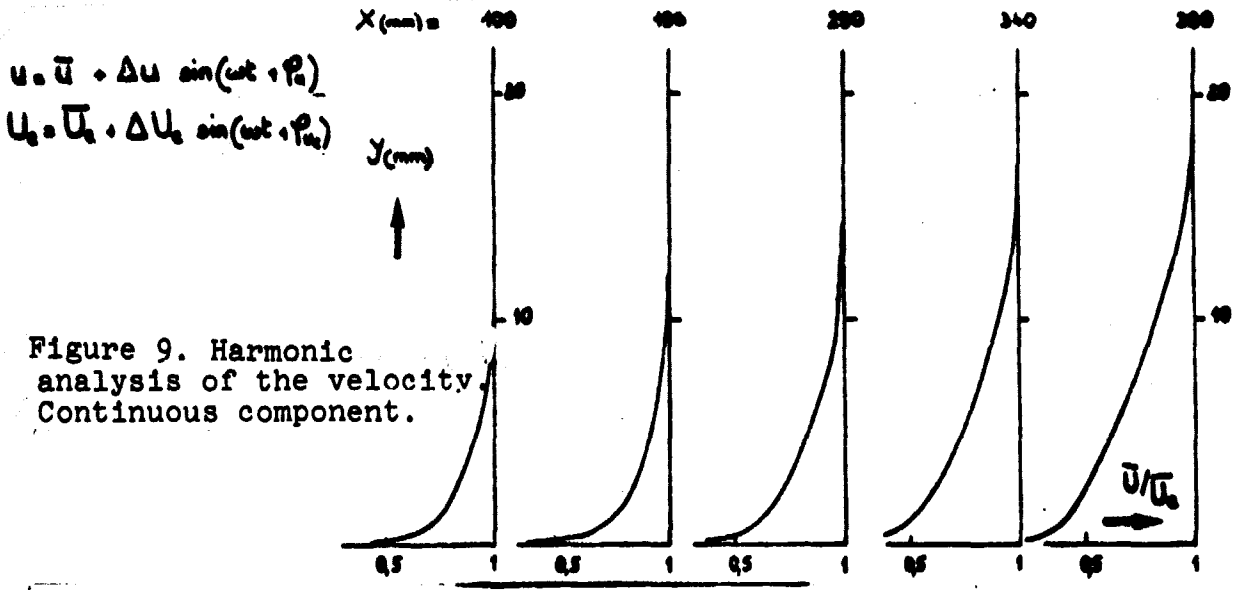

Figure 9. Harmonic analysis of the velocity. Continuous component.

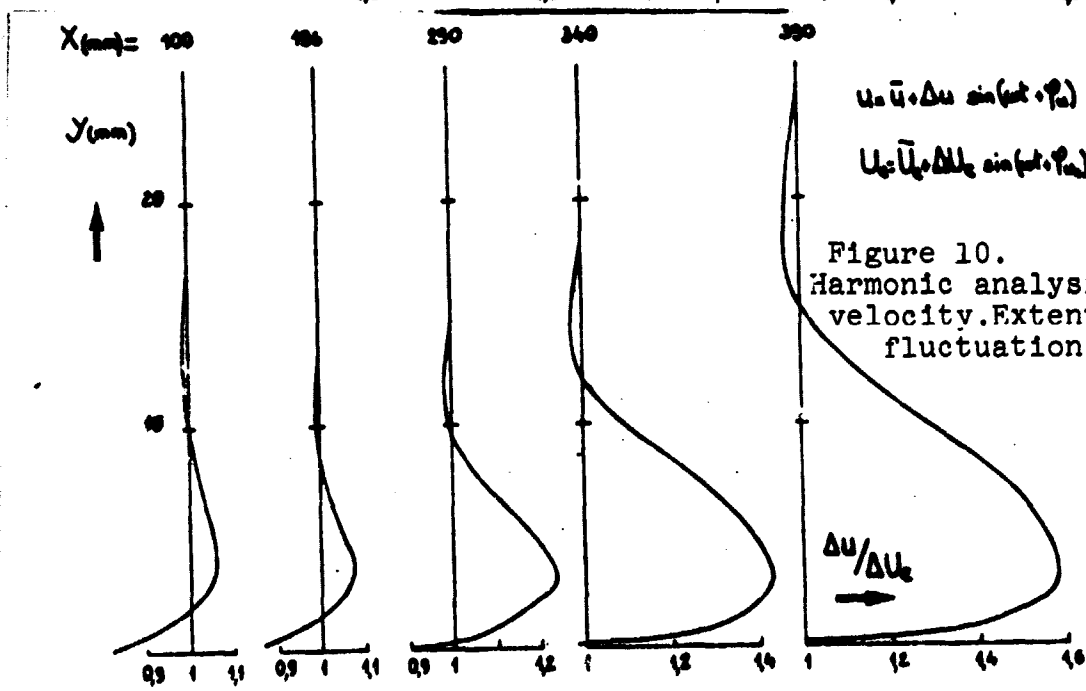

Figure 10. Harmonic analysis of the velocity. Extent of fluctuation.

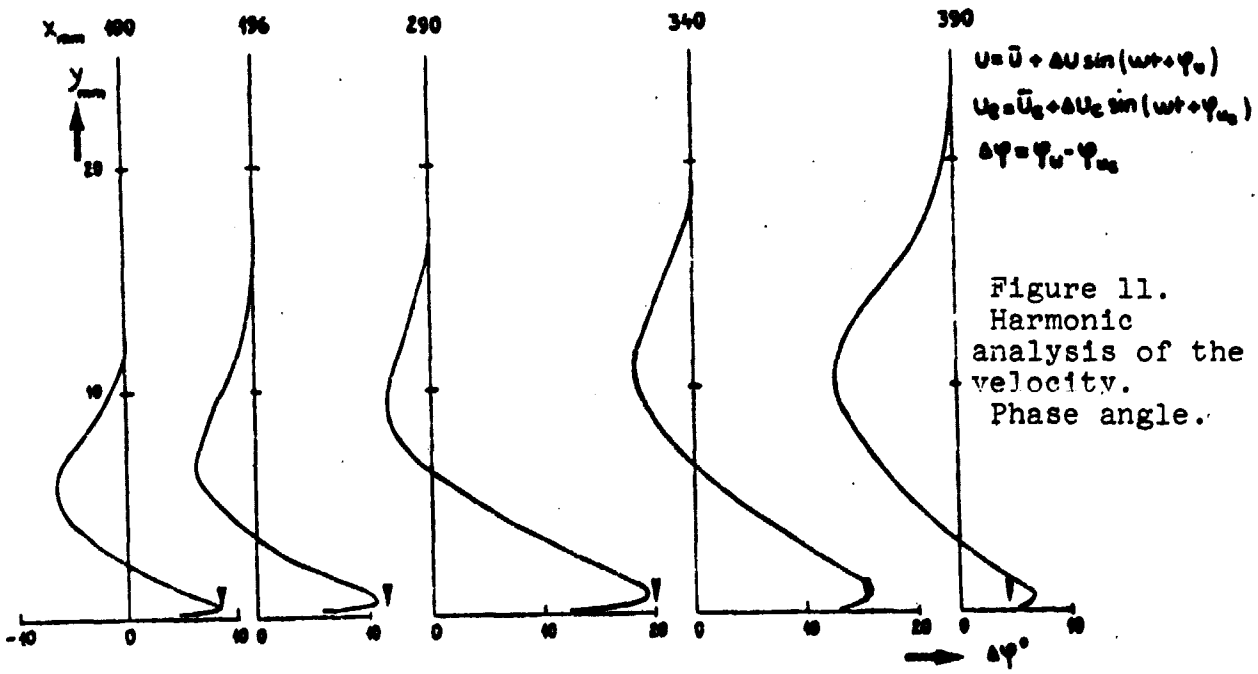

Figure 11. Harmonic analysis of the velocity. Phase angle.

certain instants, 17-21, the mean velocity direction is reversed near the skin. The return flow region, which takes up 13% of the boundary layer thickness, is perfectly visible on the corresponding profiles. At instants 5 and 9 the pattern of the profile is characteristic of a retarded boundary layer. At instant 1 it assumes an intermediary shape having a less standard pattern. It may also be observed that the variation is smaller for the thickness of the boundary layer during the cycle, which seems quite surprising if one recalls that the displacement thickness varies almost by a factor 2.

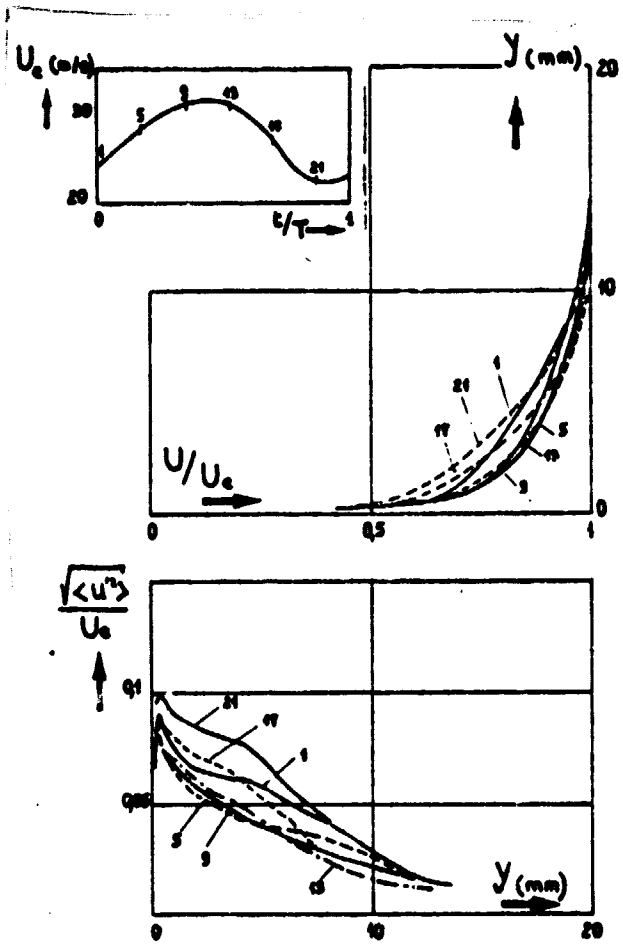

Figure 12. Profiles of velocity and turbulence at X = 240 mm.

The question arises here for this station whether or not at instant 17-21, the boundary layer is separated. Contrary to the steady case, in fact the separation does not correspond to the point where the friction is reduced to zero and where it is very possible to have a negative mean velocity near the skin without the boundary layer being separated (14-5). Theoretical studies on laminar flows (13) or numerical studies for turbulent cases (11-5) demonstrate that the unsteady separation must be combined with a fast thickening of the boundary layer. Such a thickening does not seem to exist in the present study. Perhaps a visualization of the boundary layer with the use of smoke would make it possible to resolve the indeterminacy about the nature of the flow.

The intensity profiles of turbulence at this station show a quite high maximum ranging between 11 and 17% of U_e, which is quite characteristic of an intense positive pressure gradient. It should be pointed

out that the high value of the turbulence rate in the external flow comes uniquely from the limitation of the accuracy of the laser anemometer. In fact, the hot wire shows an external turbulence close to 1% of U_e at this station. Finally it may be stated that a substantial harmonic rate on the external velocity exists and this perhaps is explained by a strong coupling between the potential flow and the boundary layer in this region.

The study of moments of order 3 and 4 of the fluctuating component of velocity contributes additional information relating to the development of turbulence. Figures 14 and 15 show the evolution of the dissymeterical factors $S = \langle u'^3 \rangle / \langle u'^2 \rangle^{3/2}$ and flattening factors $F = \langle u'^4 \rangle / \langle u'^2 \rangle^2$ at two locations of the probe and at various instants in the cycle. The evolution of these two parameters makes it possible to define the state of the distribution function u' related to a Gauss curve for which S = 0 and F = 3. Near the skin, at the station X = 100 mm, X is moderately negative but remains near 0 whereas F is about 3. The distribution function of u' must therefore not vary very much from a Gaussian distribution. This has already been observed in the case of steady boundary layers and unsteady flat plate configurations (4). This is not the case at station X = 604 mm and especially at instant 21 which corresponds to a value close to 4.4 of the shape parameter, therefore to a return flow profile. Compared to a Gauss curve, the distribution u' near the skin is longer with a peak on the side of negative values of the velocity fluctuation.

/9

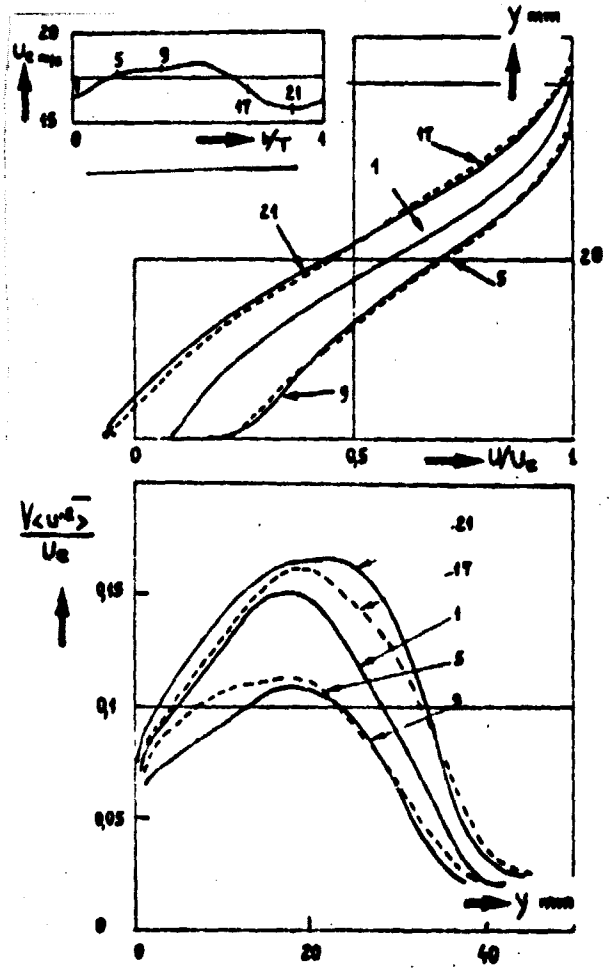

Figure 13. Profiles of velocity and turbulence at X = 604 mm.

On the outside of the boundary layer it may be observed that the dissymetrical factor becomes strongly

negative and that the flattening factor increases, and this is shown on the u' histogram by a larger peak on the side of the positive velocity fluctuations. This contributes some knowledge concerning the motion of the three zones of the boundary layer. The location of this zone has a random size, of which the distribution function is called the intermittance factor; provided that some assumptions are made, the intermittance factor γ is computed simply from the flattening factor by the relationship $\gamma = 3/F$; at a given instant $\gamma(y)$ represents the probability for which the zone of the boundary layer is farther from the wall. The curve variations of γ corresponds to a mean motion of the boundary layer zone induced by the flow pulsation. The amplitude of this forced oscillation of the free zone, related to the mean thickness of the boundary layer, is greater than X = 100 mm than at the station where negative velocities are present. In the external flow, a Gaussian distribution of turbulence is found again.

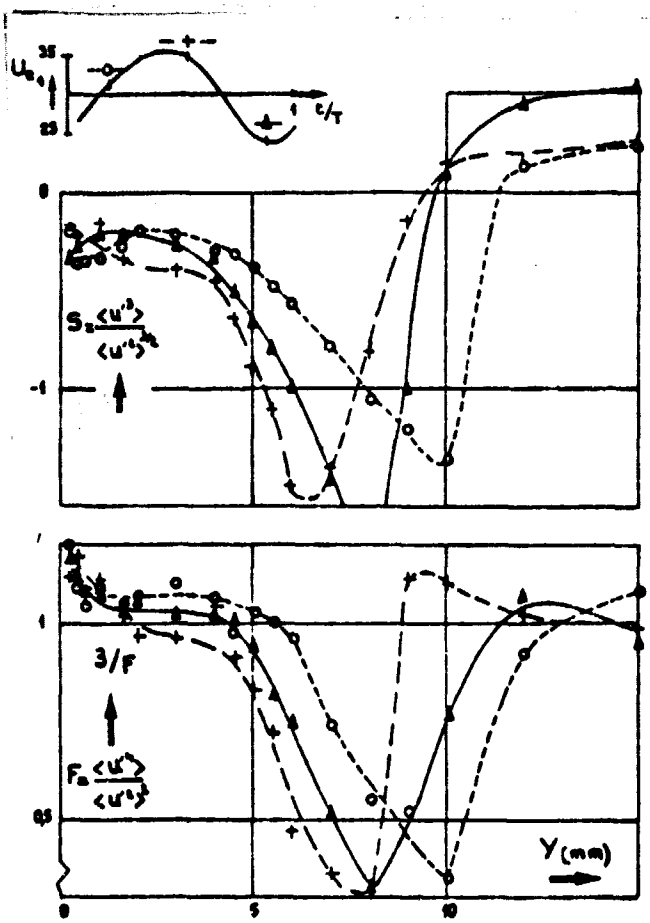

Figure 14. Factor of dissymetry and flattening X = 100 mm.

In the region where a return flow exists at certain instants, it is important to know the probability so that at a specified instant the velocity is negative. The curves on Fig. 16 show this probability as a function of the distance from the skin at various points of the maximum of the shape parameter H. When H increases, the zero friction point goes back upstream, whereas it displaces in the direction of the mean flow when H decreases. Qualitatively the curves corresponding

to the instants where the point $C_f = 0$ reverses (t = 21,23,25) are very similar to the ones obtained in the case of unsteady separation [6]. This in no longer the case when the point $C_f = 0$ goes back upstream. It is observed that the negative velocities seem to be located closer to the skin at instants 13 and 15. This is more clearly obvious on Fig. 17 where there are plottings of the isoprobability lines for a negative velocity as a function of X and y at various instants. The negative velocities take up a thin region near the skin when the zero friction point goes back up the flow (instants 15 and 17). On the other hand, this region is thicker when the point $C_f = 0$ recedes (instants 21-23). The slope of the isoprobability lines is then much higher.

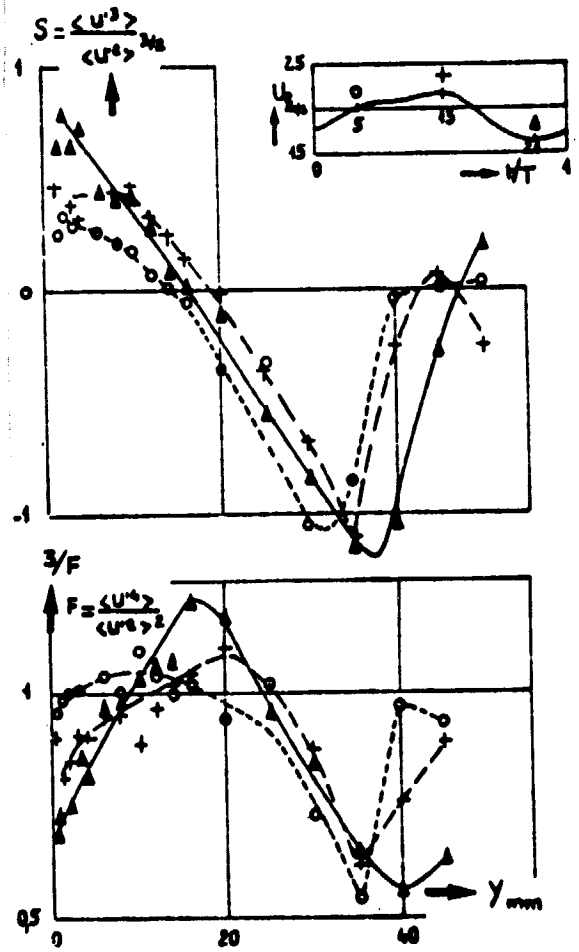

Figure 15. Factor of dissymmetry and flattening at X = 604 mm.

According to the first results of our study, it doesn't seem that the unsteady characteristic of the flow profoundly modifies the behavior of the boundary layer subjected to a positive mean pressure gradient which is quite intense. For example the mean velocity profiles have standard patterns, as is also the case for the instantaneous profiles of turbulence. In order to define this first conclusion which is somewhat subjective, we shall now attempt to analyze the experimental results already shown through the use of similarity solutions. /10

4 - ANALYSIS OF EXPERIMENTAL RESULTS. SIMILARITY SOLUTIONS.

4.1. - Determinting the similarity solutions

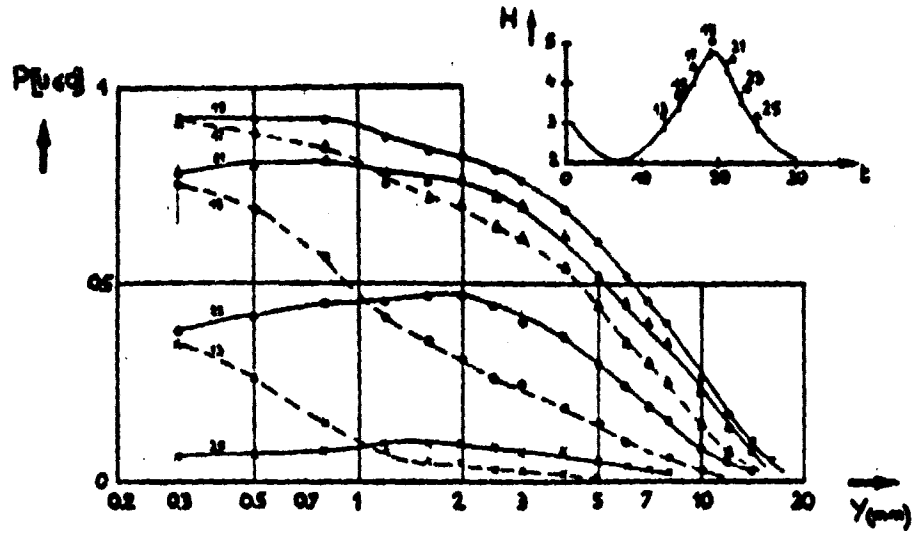

Figure 16. Profiles of probability of having negative velocities at X = 604 mm.

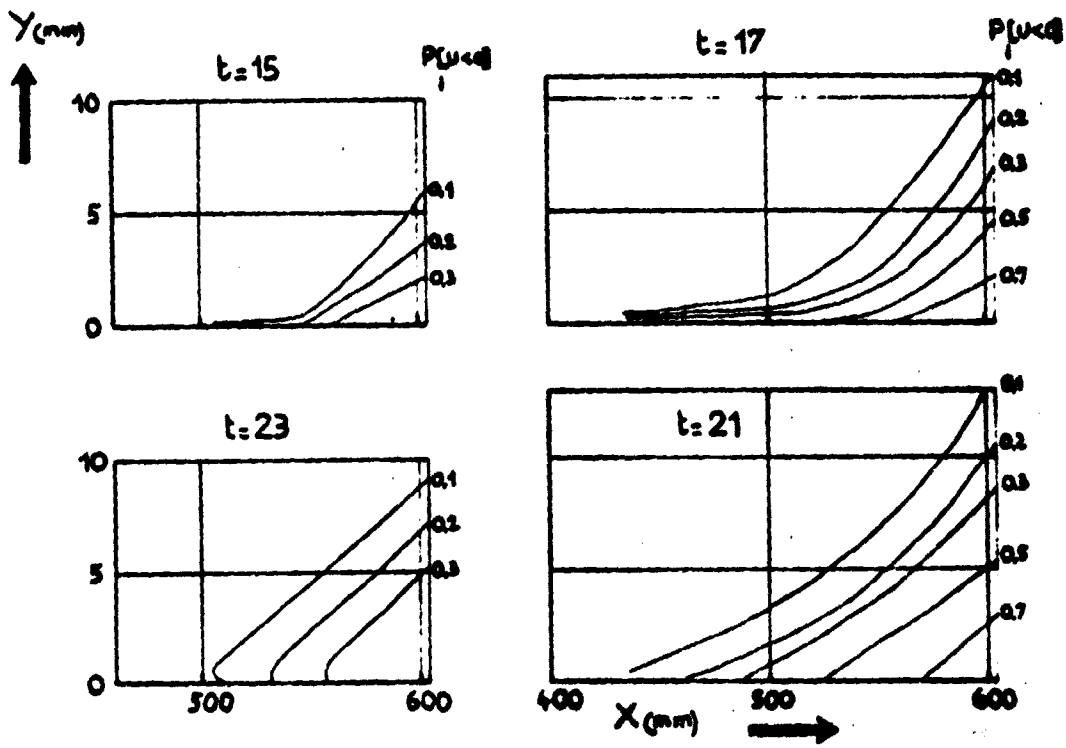

Figure 17. Charts of isoprobability of having negative velocities

The theory of connected asymptotic solutions shows that if the Reynolds number moves toward infinity, it is possible to distinguish two regions in the boundary layer:

- The region of the skin in which the phenomena depend mainly on the friction of the skin and on the viscosity and where the variables used are:

$$U^+ = U/U_\tau \text{ et } y^+ = y u_\tau/\nu \text{ with } u_\tau = u_e\sqrt{c_f/2}$$

- External region in which the friction is due uniquely to the turbulence and for which the flow is considerable for external conditions and especially for the pressure gradient. In this region the variables are used:

$$F' = \frac{u_e - U}{u_\tau} \text{ and } \eta = \frac{y}{\delta}$$

As the Strouhal numbers for flows which we consider not to be too high, we shall simply assume that the law of this skin defined in its state remains valid. This leads then to the overlapping regions, i.e. where y^+ moves toward infinity and η moves toward zero, at a velocity profile represented by a logarithmic law: /11

$$U^+ = \frac{1}{\chi} \ln y^+ + 5{,}25 \text{ with } \quad \chi = 0{,}41 \tag{1}$$

To determine the velocity profile shape in the external region we are making the assumption that the adverse velocity profile $F' = (u_e - U)/u_\tau$ is a function uniquely of y/δ, this is a similarity assumption, δ being the standard thickness of tne boundary layer function of x and t:

$$\frac{u_e - U}{u_\tau} = F'(y/\delta) \tag{2}$$

Since the Reynolds number moves toward infinity, the viscous friction $\mu\, \partial U/\partial y$ can be omitted in the presence of the Reynolds stress $-\rho\langle u'v'\rangle$ this stress is expressed simply by using a combined length model (10):

$$\tau = -\rho\langle u'v'\rangle = \rho\, l^2 \left(\frac{\partial U}{\partial y}\right)^2 \tag{3}$$

with $$\frac{l}{\delta} = 0{,}085 \tanh\left(\frac{\chi}{0{,}085}\frac{y}{\delta}\right)$$

By using the similarity assumption (2) in the turbulence diagram, we can write the local equation for the quantity of motion for the variable F'. The assumption of an infinite Reynolds number makes it possible to expand this equation in relation to the small parameter $\gamma = \sqrt{c_f/2}$. We shall select only the terms of order $\sqrt{c_f/2}$; we thus have:

$$\frac{\nu}{\tau_p}\left(\frac{\rho}{\delta}\right)^2 F''^2 = 1 + (\eta F' - F)\left(\frac{1}{\gamma u_e}\frac{\partial \delta}{\partial t} + \frac{1}{\gamma}\frac{\partial \delta}{\partial x} - \beta_x\right) + \beta^* F$$

$$F'' = \frac{dF'}{d\eta} \qquad F = \int_0^\eta F' d\eta \qquad \eta = \frac{y}{\delta(x,t)} \tag{4}$$

with $\beta^* = \beta_t + 2\beta_x \qquad \beta_x = -\frac{\delta}{\gamma u_e}\frac{\partial u_e}{\partial x}$

$\gamma = (c_f/2)^{1/2} \qquad \beta_t = -\frac{\delta}{\gamma u_e^2}\frac{\partial u_e}{\partial t}$

with the boundary conditions: $\eta = 0$ and $F' = 0$ in $\eta = 1$ leading to the relationship:

$$\frac{1}{\gamma u_e}\frac{\partial \delta}{\partial t} + \frac{1}{\gamma}\frac{\partial \delta}{\partial x} - \beta_x = \frac{1}{F_1} + \beta^* \tag{5}$$

with $F_1 = \int_0^1 F' d\eta$

and equation (4) is finally put in the form:

$$\left(\frac{\rho}{\delta}\right)^2 F''^2 = 1 - \frac{F}{F_1} + P\eta F' \tag{6}$$

with $P = \frac{1}{F_1} + \beta^*$

The local equation of the quantity of motion has thus become a common differential equation for the adverse velocity F_1. Its solution does not depend only on the parameter β^* as F_1 is determined when the solution is known. The only modification relating to the steady case is the substitution of the parameter $2\beta_x$ by $\beta_t + 2\beta_x$. This means that the family of profiles obtained in the unsteady state is the same as that obtained for the steady case parametered by using $\beta_t + \beta_x$ and not $2\beta_x$.

4.2. - Analysis of the Similarity Solutions

The parameter β^* does not allow analysis of the family of profiles, as it is directly related to the local gradient of external velocity which is usually incompatible with the existence of a similarity law which implies that β^* must be constant, therefore independent of x and t; this is a condition which is not rigorously fulfilled except for the boundary layer in equilibrium. In general it is preferred to use as a parameter of the family of profiles a quantity which characterizes the shape of the profiles themselves. We have selected the Clauser factor defined by:

$$G = \int_0^\infty F'^2 d\eta \Big/ \int_0^\infty F' d\eta$$

By definition $F' = (Ue - U)/U\tau$ will have the following relationships:

(7)

$$G = (H-1)/H\gamma$$

$$\delta_1/\delta = \gamma F_1$$

(8)

where F_1 is a function of G determined by the similarity solutions which are represented analytically by the formula:

$$F_1 = 0{,}6136 - (3{,}5 + 4{,}66(1/6 - 0{,}444)^2)/6$$

In order to be able to compare the experimentally measured profiles to the profiles deduced from the similarity solutions, it is necessary to use a law of friction to determine the parameter $\gamma = \sqrt{\theta_1/\ell}$. This law is obtained simply by overlapping the skin law for $y^+ \to \infty$ and the law of adverse velocity for $\eta \to 0$. The similarity solutions show that when $\eta \to 0$ adverse velocity profiles follow a logarithmic law of the shape:

$$F' = \frac{U_e - U}{U_\tau} = \frac{1}{\chi} L_n \frac{y}{\delta} + D(G) \qquad (9)$$

where D is a function of G, determined by these solutions.

The relationship (8) and the law of the skin (1) lead to the friction law:

$$\frac{1}{\gamma} = \frac{1}{\chi} L_n \frac{\gamma u_\tau \delta}{\nu} + 5{,}45 + D$$

assuming (10) $$\frac{1}{\gamma} = \frac{1}{\chi} L_n \frac{u_\tau \delta_1}{\nu} + 5{,}45 + D - \frac{1}{\chi} L_n F_1 \qquad (10)$$

$D^* = 5.25 + D - (1/x)\, L_n\, F_1$ is a function of G which may be computed from the similarity solutions and represented analytically by the expression:

$$D^* = 2G - 4{,}25\, G^{1/2} + 2{,}12 \qquad (11)$$

The relationship (7) combined with the friction law (10) permits the determination of the Clauser parameter G of a given experimental profile if H and δ_1 are known. In figure 18 a comparison is provided of the experimental profiles obtained at various instants in the cycle with profiles deduced from the similarity solutions and corresponding to the samevalue of the parameter G. It may be stated that a good overall agreement exists, including one for the profiles of which the shape parameter is quite high, of order 2. We may then conclude that the unsteady profiles may be represented by a profile family for a parameter, even for boundary limits subjected to intense positive pressure gradients.

The presence of a logarithmic region for velocity profiles /12 is shown in Fig. 19. The coefficient of friction present in the logarithmic law (1) was determined to have the best possible agreement. It may be stated that as with a steady flow, the extent of the logarithmic

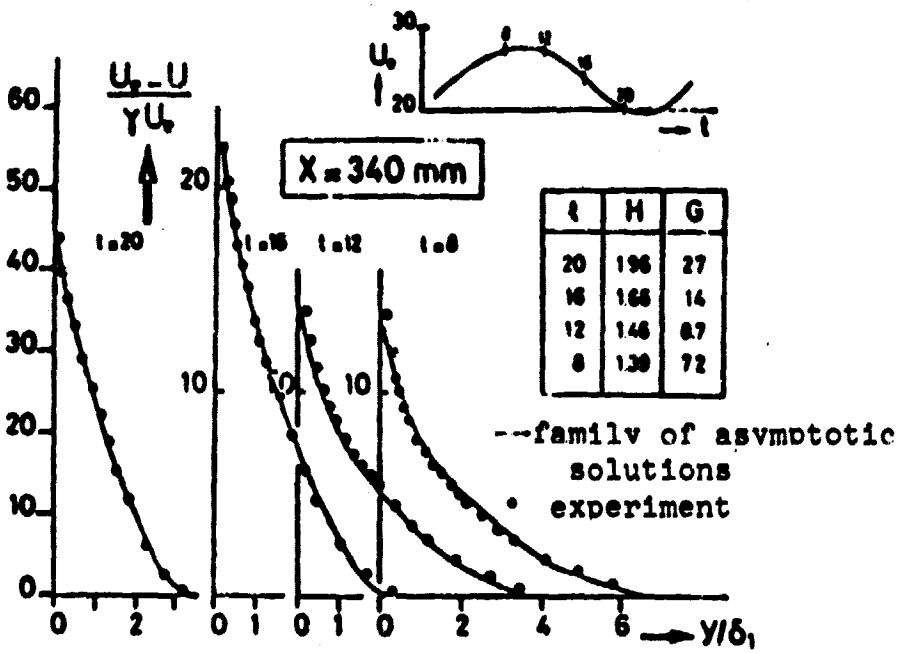

Figure 18 - Adverse velocity. Comparison with a family of similar solutions.

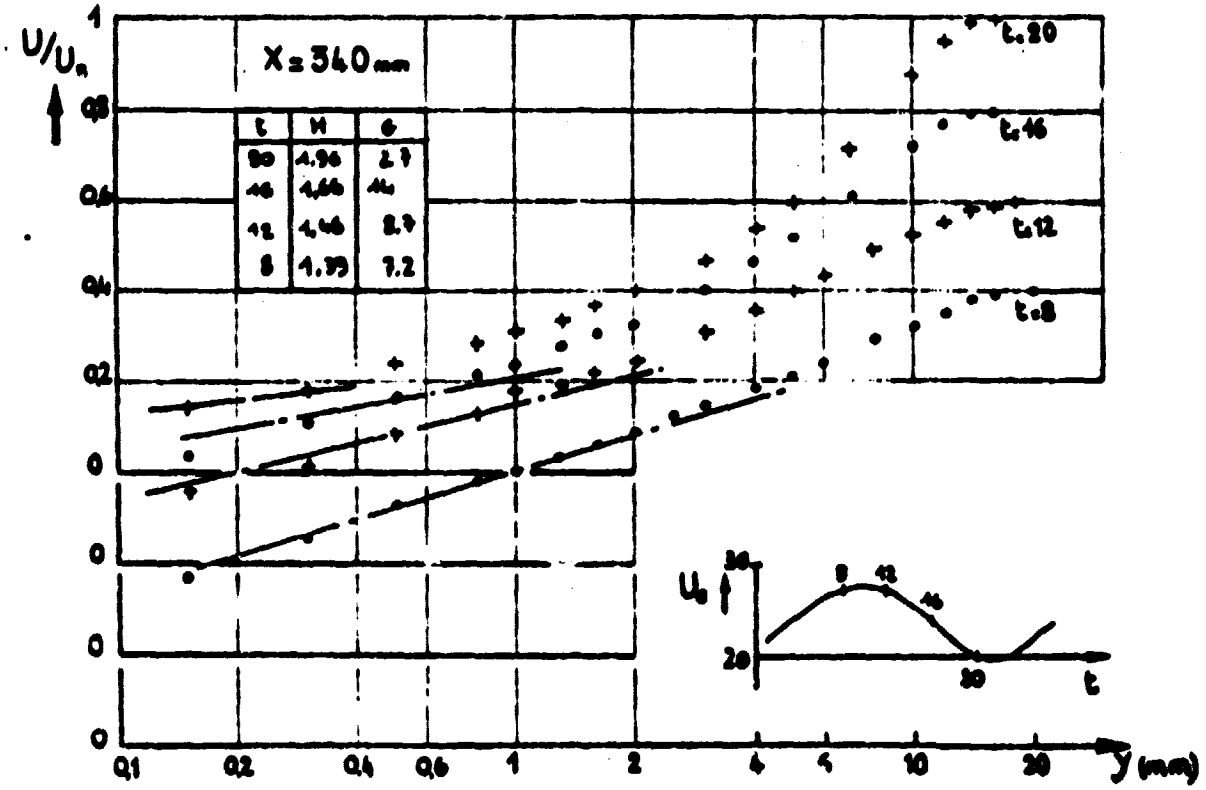

Figure 19 - Logarithmic law of velocity.

region decreases as the shape parameter increases, while the experimental Reynolds number remains finite.

4.3. - Development of the logarithmic law. Calculation of the phase angle.

The existence of a friction law (10) and of a logarithmic velocity profile in the overlapping region (1) permits the calculation of the phase angle for velocity in this region. For that we make the assumption of small perturbations, i.e. we assume that the amplitude of the various values present in these relationships remains small, which must be the case if the amplitude of the external velocity fluctuations is not too high. We have then:

$$u_e = u_{e_0} + u_{e_1} e^{i\omega t}$$

$$U = U_1 + U_1 e^{i\omega t} \qquad u_{e_1}/u_{e_0} \ll 1$$

where only U_1 is complex. Adding these developments together with /13 those of γ, H, θ, δ_1 and G in the relations (1) (10), we obtain the following expression for velocity in the logarithmic region:

$$U = \gamma_0 u_{e_0} \left(\frac{1}{\chi} \ln \frac{y u_{e_0}}{\nu} + 5{,}45 \right)$$
$$+ \gamma_1 u_{e_0} \left(\frac{\gamma_1}{\gamma_0} + \frac{u_{e_1}}{u_{e_0}} \right) \left(\frac{1}{\chi} \ln \frac{y u_{e_0}}{\nu} + \frac{1}{\chi} - 5{,}45 \right) e^{i\omega t} \qquad (12)$$

We see then that the phase angle of velocity in this region is independent of y and is equal to the phase of $\gamma_1/\gamma_0 + U_{e1}/U_{e0}$, which is also the phase of $\gamma u_e = \sqrt{\tau_p/\rho}$. The velocity phase in the overlapping region is therefore constant and equal to that of the parietal friction.

Based on the law of friction (10), on relation (7) and on making an estimate of the small perturbations, we obtain for the phase velocity the expression:

$$\operatorname{tg} \varphi_u = \frac{(C+D) \frac{\Delta \delta_1}{\Delta u_e} \sin \varphi_{\delta_1} - D \frac{\Delta \theta}{\Delta u_e} \sin \varphi_\theta}{(C+1) + (C+D) \frac{\Delta \delta_1}{\Delta u_e} \cos \varphi_{\delta_1} - D \frac{\Delta \theta}{\Delta u_e} \cos \varphi_\theta} \qquad (13)$$

where ΔU_e, $\Delta \delta_1$, $\Delta \theta$ representing the fluctuation amplitudes of U_e, δ_1 and θ and where the coefficients C and D do not only depend on the mean flow:

$$C = \frac{Y_4}{\chi A} \qquad D = \frac{B}{A}$$

with

$$A = \left(2 - 4{,}25/2\sqrt{C_4}\right)(H_4 - 1)/H_4 - 1$$

$$B = \left(2 - 4{,}35/2\sqrt{C_4}\right)/H_4$$

The phase angle which is thus calculated is represented by the arrows on Fig. 11 for several experimental profiles. It corresponds to a maximum of the phase angle located in the logarithmic region. The values of y^+ which correspond to this maximum are included, for the various profiles represented, between 30 and 100. Experimentally, it may be stated that the phase angle decreases near the skin which does not seem very concordant with the fact that the parietal friction phase must be equal to that of the velocity in the logarithmic region. To eliminate this difficulty we must assume that the flow of velocity in the sub-layer is not unique but is a function of time. We must in any case insist on the difficulty arising when measuring a phase angle requiring an accuracy of several degrees. Moreover, the decline in the phase occurs very close to the skin, in a region where it is not excluded that a certain interaction of the skin on the thermic field of the hot wire exists. The measurements computed with the laser anemometer nevertheless confirm the results observed. This difficulty shows the importance of a detailed study of the sub-layer, unfortunately impossible to carry out in the present case due to the limited thickness of the boundary layer.

A comparison between the measured values and calculated values of the phase angle of velocity is shown in Fig. 20 for the experiments presented. The two points shown in black which deviate from the first bisecting section correspond to the stations where at certain instants there is a return flow. Their dispersion should not be surprising, since the law of friction loses its meaning when the parietal friction reduces to zero. We have also reported

in this figure the results obtained by M.H. Patel [12] for a configuration in which the external flow perturbation is displaced considerably by the mean flow velocity:

$$U_e = U_0 + U_1 \sin \omega\left(t - \frac{x}{a}\right) \text{ with } a > U_e$$

In such a configuration the instantaneous pressure gradient is created both by time derivatives and in X of the external velocity. Experimentally, we have considerably larger phase angles which are quite predictable by the present calculations. Let us note that in the case of the Patel study, there was no decline in the phase near the skin.

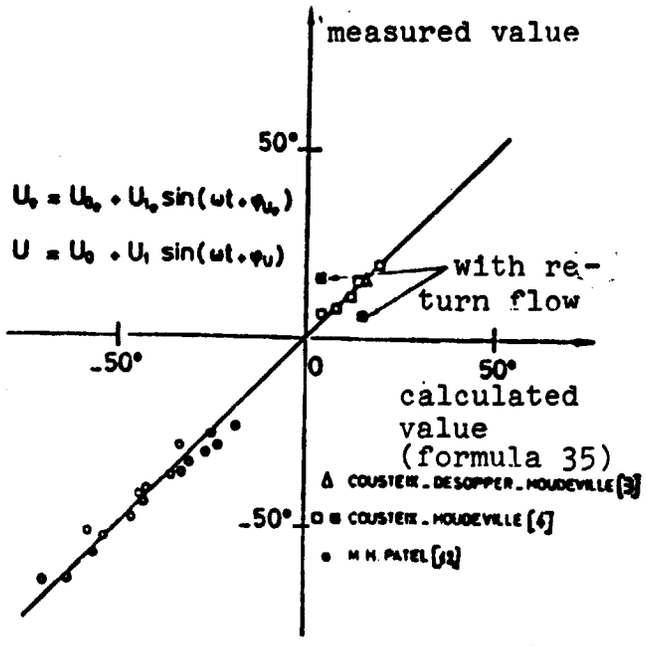

Figure 20 - Phase angle calculation. Comparison with the experimental case.

4.4. - Integral Method. Application to the experimental case.

We have seen that the experimental profiles obtained at various instants in the cycle are correctly represented by a family of profiles, with only one parameter, deduced from similarity solutions. This permits the use of a simple integral method to calculate the unsteady flows which may lead to separation of the boundary layer. Such a method has already given good results in the case of isolating boundary layers on a flat plate configuration [3-4]. We shall recall briefly its principles.

The overall equations of continuity and quantity of motion are integrated step by step over time. These equations are written in the incompressible case:

$$\frac{\partial \delta}{\partial x} - \frac{v_e}{u_e} = \frac{1}{u_e}\frac{\partial}{\partial x}u_e(\delta - \delta_1) \tag{14}$$

$$\frac{C_f}{2} = \frac{\partial \theta}{\partial x} + \theta\frac{H+2}{u_e}\frac{\partial u_e}{\partial x} + \frac{1}{u_e^2}\frac{\partial}{\partial \theta}(u_e \delta_1) \tag{15}$$

δ is the thickness of the boundary layer and is placed in a steady state:

$$\delta_1 = \int_0^\delta \left(1 - \frac{u}{u_e}\right) dy \qquad \theta = \int_0^\delta \frac{u}{u_e}\left(1 - \frac{u}{u_e}\right) dy$$

$$H = \delta_1/\theta \qquad C_f/2 = \tau_e/\rho_e u_e^2$$

The five unknowns which appear in the system $(\partial\delta/\partial x = v_e/u_e,\ C_f,\ \delta_1,\ \theta,\ \delta)$ /14 are estimated by using additional relationships deduced from the similarity solutions already presented.

CALCULATION OF THE DRIVE COEFFICIENT

This coefficient, having the shape $\partial\delta/\partial x - v_e/u_e$, appears in the overall equation of continuity. It may be calculated from the local equation of continuity by making an assumption of similarity and by using the small parameter $\gamma = \sqrt{C_f/2}$ which was already used for the equation of speed momentum. We have then the relationship:

$$v/u_e = \gamma\beta x \eta \tag{16}$$

which permits the expression of vertical velocity V.

At the external zone of the boundary layer we have then:

$$v_e/u_e = \gamma\beta x \tag{17}$$

The drive coefficient is expressed then from this relationship and from (5) in the form:

$$\frac{\partial \delta}{\partial x} - \frac{v_e}{u_e} = P\gamma - \frac{1}{u_e}\frac{\partial \delta}{\partial t} \tag{18}$$

where P is a function of G which results from the similarity solutions and which has been represented by the relationship:

$$P = 0{,}074\,G - 1{,}0957 / G \qquad (19)$$

In comparison with the steady case, it may be observed that an additional term is added in this drive coefficient: $-\frac{1}{U_e}\frac{\partial \delta}{\partial t}$

The other closure relationships of global equations have been obtained in paragraphs 3.2. This is the law of friction (10) and of relationships (7) and (8) deduced directly from the definition of the adverse velocity profiles. It is recalled that these relationships are:

$$\frac{1}{\gamma} = \frac{1}{\chi} \ln \frac{U_e \delta_1}{\nu} + \mathcal{D}^*(\theta)$$

$$\frac{\delta_1}{\delta} = \gamma F_1$$

$$G = \frac{H-1}{H\gamma}$$

The integration of the global equations of momentum and of continuity (14) (15) to which the closure relationships may be added requires knowledge of the boundary conditions. We must know the external velocity as a function of X at each instant and at the initial conditions of the boundary layer: at instant t = 0 it is necessary to know the state of the boundary layer as a function of X and by giving, for example, the distribution of δ_1 and θ. In the case of a periodic flow this condition does not affect the result, the latter also becomes periodic after a sufficient period of calculation. The other initial condition deals with the given boundary layer in X = 0 and at each instant. This assumption is important, because in the steady state the accuracy of the estimates may depend on it.

The integral method which we have described has been applied to the experimental case presented. The external velocity is introduced from the harmonic analysis, limited to the second term, of the experimental distribution of velocity. The data of δ and θ as a function of time at the first point of calculation in X are also deduced from the harmonic analysis of integral thicknesses measured.

Figures 21 and 22 demonstrate the estimated development of the displacement thickness δ_1 and of the shape parameter H represented by their harmonic analysis. The relative amplitudes of the fluctuation of H and of δ_1 are related to those of the external velocity.

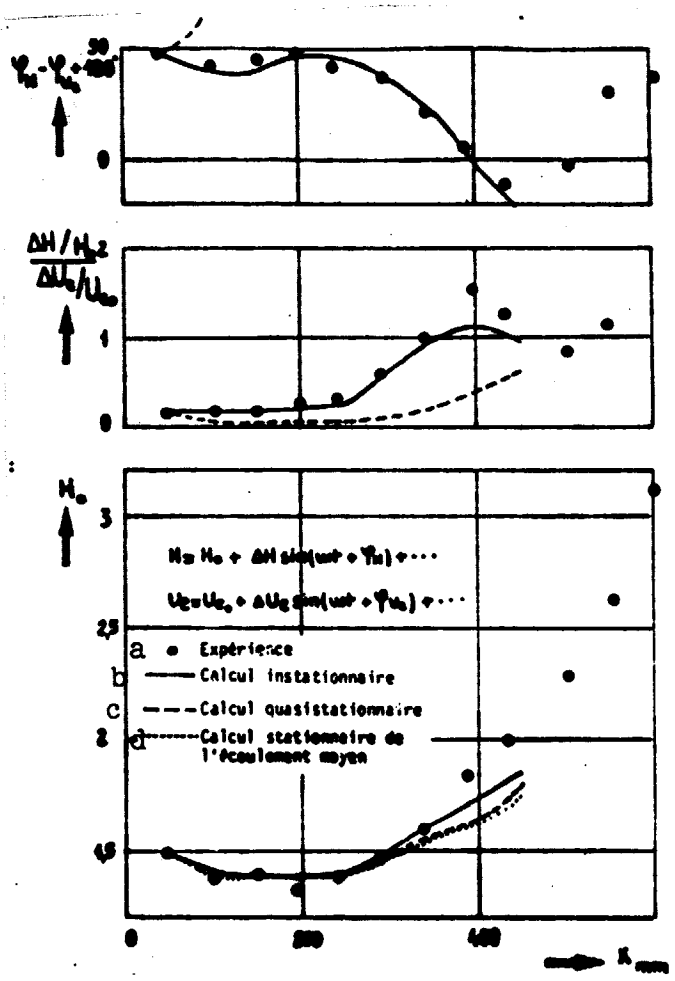

Key:

a) Experiment
b) Unsteady measurement
c) Quasisteady measurement
d) Steady measurement of the mean flow

Figure 21. Harmonic analysis of the shape factor. Measurement - experiment.

The measurement does not exceed the station X = 450 mm, since downstream from this point begins a return flow which implies the transmission of data from the downstream toward the upstream end and thus requires knowledge of the additional boundary conditions at certain instants. A more detailed discussion and careful study of this problem relating to these boundary conditions is presented in [5].

The evolution of mean values has been determined from a steady measurement for the mean flow. The small difference between this measurement and the unsteady measurement confirms what has already been observed experimentally, namely the small effect of the unsteady state on the development of the mean flow, an effect which is due essentially to the nonlinear terms of the equations. We must nevertheless point out that this effect becomes more important as the shape parameter increases, i.e. when we come near a region with return flow.

To determine the importance of these unsteady effects in the configuration under study, we present also a quasi-steady measurement. This consists of a definition at each instant of the boundary layer development by a steady method but by applying the natural velocity /15 distribution which exists at this instant. This means that the unsteady terms will be omitted in the equations. The developments which are thus calculated from the various values deviate considerably from those measured or calculated by the unsteady method. This is particularly obvious for the fluctuating values.

The deviations which appear between the unsteady calculation and the experimental results relate to the evolution of the fluctuation amplitudes or to the phase angle of δ_1 and H does not seem very large, if account is taken of the difficulty in measuring these values with a good accuracy. If it is assumed, for example, that there is an accuracy of 3% on the measurement of δ_1 and 1% on that of U_e, the accuracy obtained on the amplitude relative to the variation of δ_1 related to that of U_e is about 20%. The accuracy of the phase angles of δ_1 and H is

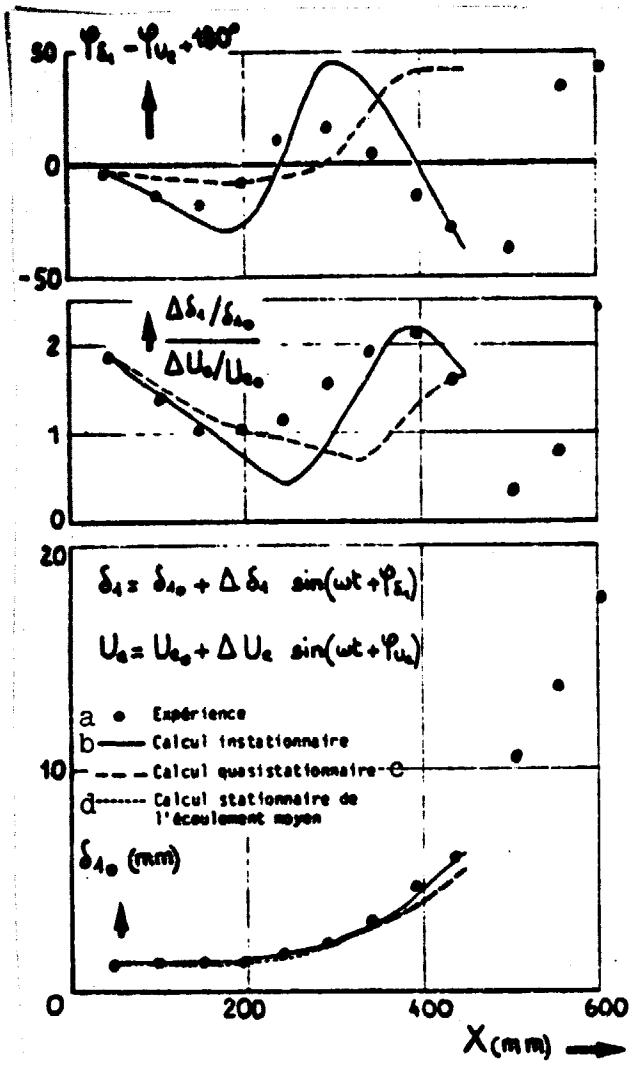

Figure 22. Harmonic analysis of the thickness of displacement. Measurement. experiment.

Key: a) Experiment
b) Unsteady measurement
c) Quasi-steady measurement
d) Steady measurement of the mean flow

more difficult to determine but must be close to 10 or 20°.

5 - CONCLUSION

The experimental study of an oscillating boundary layer subjected to a quite high mean pressure gradient resulting in separation demonstrates that the development of the boundary layer is not profoundly modified by the unsteady characteristic of the flow. This result extends to the new case which we have obtained during this study of the flat plate configuration, always for moderate Strouhal numbers. We may nevertheless conclude with certainty that this study is not completed. In fact, if the measurements of mean velocity, in the sense of overall average, as well as of the longitudinal turbulence component have been performed up to a point where the return flows exist and even beyond that due to the use of a laser velocimeter, we have available for the present time no information about a value which is as important as the turbulent friction $\langle u' v' \rangle$. This shall be dealt with in the study that follows.

Comparison of the experimental profiles of velocity with the profiles deduced from the similarity solutions shows a good agreement, including for those high values of the shape parameter close to 2.

The existence of a logarithmic region is also brought to light. The development by a method of small perturbations of this logarithmic law gives important results relating to the shape of the phase angle profiles of velocity in the boundary layer and permits an accurate estimate to be made of the maximum phase angle.

Finally, an unsteady integral method using the global equations of momentum and of continuity together with the closure relationships deduced from the similarity solutions, makes it possible to predict quite accurately the development of the boundary layer in the configuration presented. Such a method is nevertheless limited to a range where there are no negative velocities, on the one hand because the closure relationships are used, and on the other hand because of the problem of the boundary conditions. The interest of such a calculation method is in its simplicity, which is important for applying practical solutions. It remains now to define its range of validity, especially for high values of the Strouhal number.

REFERENCES

1. Boutier, A., "Compact velocimeter for measurements in very turbulent flows," ONERA, N.T. No. 237 (1974).

2. Boutier, A., Lefevre, J., Fertin, G.,Appel, J.,"Report on the use of the one dimensional laser velocimeter," ONERA, R.T. No. 13/1883 PN, 28 April 1977.

3. Costeix, J., Desopper, A., Houdeville, R., "Research on the unsteady boundary layers," La Rechereche Aerospatiale, No. 1977-3, pp. 167-177.

4. Costeix, J., Desopper, A., Houdeville, R., "Structure and development of a turbulent boundary layer in an oscillatory external flow," Report presented to the Symposium Turbulent Shear Flows, University Park, Pennsylvania, April 18-20, 1977, ONERA, T.P. No. 1977-14.

5. Cousteix, J., Houdeville, R., "Turbulent boundary layer calculations in unsteady flow. Numerical Methods in Applied Fluid Dynamics," University of Reading, January 4-6, 1978.

6. Cousteix, J., "General view of research on boundary layers in oscillating flow," 15e Colloque d'Aerodynamique Appliquee, Marseille 7-9 November 1978.

7. McCroskey, W.J., "Some current research in unsteady fluid dynamics," The 1976 Freeman scholar lecture. Journal of Fluids Engineering, 99, March 1977.

8. Eichelbrenner, E.A., "Research on unsteady boundary layers," Proc. of the IUTAM Symp. Quebec 1971.

9. Karlsson, S.K.F., "An unsteady turbulent boundary layer," J. Fluid Mech., 5, 1959, pp. 622-636.

10. Michel, R., Quemard, C., Durant, R., "Application of a diagram for the mixing length of the study on turbulent boundary layers in equilibrium," ONERA, N.T. No. 154 (1969).

11. Nash, J.F., Patel, V.C., "Calculations of unsteady turbulent boundary layers with flow reversal," NASA-CR-2546 (1974).

12. Patel, M.H., "On turbulent boundary layers in oscillatory flows," Proc. R. Soc. Lond. A. 353, 121-144, (1977).

13. Shen, S.F., Nenni, J.P., "Asymptotic solution of the unsteady two-dimensional incompressible boundary layer and its implications on separation," Symposium on Unsteady Aerodynamics, Kinney, R.B., ed., Univ. Arizona, Tucson, 1975, pp. 245-259.

14. Telionis,D.P., "Unsteady boundary layers. Separated and attached." AGARD Conference on "Unsteady Aerodynamics," Ottawa 26-28 Sept. 1977.

15. Telionis, D.P., "Calculation of time dependendant boundary layers," Unsteady Aerodynamics, Vol. 1, ed. Kinney, R.B., (1975) pp. 155-190.

16. Simpson, R.L., Strickland, J.H., Barr, P.W., "Features of a separating turbulent boundary layer in the vicinity of separating," J. Fluid Mech. Vol. 79, pp. 553-594 (1977).

17. Simpson, R.L., "Features of unsteady turbulent boundary layers as revealed from experiments," AGARD Conference on "Unsteady Aerodynamics," OTTAWA 26-28 Sept. 1977.